Application of the Quantum-Point-Contact Formalism to Model the Filamentary Conduction in Ta_2O_5-Based Resistive Switching Devices

Jaime M.M. Andrade,[1] Carlos M.M. Rosário,[1,*] Stephan Menzel,[2] Rainer Waser,[2,3,4] and Nikolai A. Sobolev[1,5]

[1] *i3N and Physics Department, University of Aveiro, Aveiro 3810-193, Portugal*
[2] *Peter Grünberg Institute 7 (PGI-7) and JARA-FIT, Forschungszentrum Jülich GmbH, Jülich 52425, Germany*
[3] *Peter Grünberg Institute 10 (PGI-10) and JARA-FIT, Forschungszentrum Jülich GmbH, Jülich 52425, Germany*
[4] *Institut für Werkstoffe der Elektrotechnik II, RWTH Aachen University, Aachen 52074, Germany*
[5] *Laboratory of Functional Low-Dimensional Structures, National University of Science and Technology MISiS, Moscow 119049, Russia*

(Received 7 September 2021; revised 20 December 2021; accepted 31 January 2022; published 25 March 2022)

Redox-based resistive random access memories (ReRAMs) are promising candidate devices for new memory and computing paradigms. However, the fundamental mechanisms that rule the conduction in these devices are still heavily debated. The present work focuses on studying one model for the conduction, the quantum point contact (QPC), and specifically a single-subband approximation (SSA) to this model. With this intent, Pt(20 nm)/Ta(15 nm)Ta_2O_5(5 nm)/Pt(20 nm) resistive switching devices are fabricated and electrically characterized by measuring current-voltage (*I-V*) curves in both resistance states. The QPC model has been found to be hard to apply, as the starting parameters have a strong influence on the fitting results. On the other hand, the SSA has proved its ability to provide good fits to the data and to do so better than other typical conduction mechanisms considered. However, its physical basis is criticized and it is concluded that in the devices studied, multiple subbands likely contribute to the conduction, in direct opposition to the assumptions made in such an approximation. A reinterpretation of the parameters of the SSA is proposed, to reconcile the increased performance with greater physical accuracy. Beyond that, the main challenges and difficulties regarding the application of the QPC to the case of valence-change-based ReRAM are discussed.

DOI: 10.1103/PhysRevApplied.17.034062

I. INTRODUCTION

Resistive switching (RS) devices display a nonvolatile reversible change in their two-terminal electrical resistance when subject to a strong electric field. Devices with this property naturally lend themselves to the development of memory technologies, called redox-based resistive random access memories, or ReRAMs [1]. These can be applied as storage-class memories (SCMs), bridging the gap between the affordability of flash memories and the low latency of dynamic RAMs (DRAMs) [2]. RS devices can also be applied as synaptic elements in neuromorphic circuits that promise faster and more efficient computing [3]. These features make the resistive switching phenomenon an active field of study. RS devices are normally composed of a metal-insulator-metal structure and usually present two states of resistance, an *off* high-resistance state (HRS) and an *on* low-resistance state (LRS). The transitions between these two states are called "SET" (high-to-low resistance) and "RESET" (low-to-high resistance). Conduction in these devices is typically filamentary in nature, with a conductive filament (CF) being formed or disrupted to turn the device *on* or *off*, respectively [1]. In metal-oxide–based RS devices, where the insulator layer is a transition-metal oxide and neither of the two metals is highly electrochemically active, the RS is normally modeled by the valence-change mechanism (VCM). According to the latter [1,4], after the electroforming step, an incomplete CF called a plug is formed between the two electrodes. This CF is interrupted at the interface with one of the electrodes, leaving a region called the disk, which acts as a barrier to electronic transmission. The electric-field-assisted migration of oxygen-related defects to or from the disk switches the cell *on* or *off*. While most of the models for VCM switching consider CFs composed of oxygen vacancies [5–8], there are also experimental observations that argue in favor of having metallic compounds in the CF, especially in Ta_2O_5-based structures [9–15]. However, the

*cmiguelrosario@ua.pt; Current affiliation: Faculty of Science and Technology and MESA+ Institute for Nanotechnology, University of Twente, 7500AE Enschede, The Netherlands.

filaments have been reported to be of nanometric dimensions [16]; thus, a direct study of their composition or structure can be a challenge. The analysis of the main conduction mechanisms present can be a way to overcome this barrier and provide valuable insight. We focus on the quantum-point-contact (QPC) model of conduction and a single-subband approximation (SSA) to this model. The QPC model [17–19] considers that the CF contains a constriction that, at its narrowest point, is smaller than the electron mean-free path. This leads to a transverse quantization of the electron energy. Around the bottleneck, the potential along the axis of the filament for the nth quantized level can be seen as the band bottom of an nth conductive channel, here referred to as subband. These subband bottoms act as barriers to conduction. Through the Landauer-Büttiker formalism [20,21], one can express the current across the constriction as

$$I = \frac{G_0}{e}\int_{-\infty}^{+\infty} T(E)\left[f_C(E) - f_A(E)\right] dE. \tag{1}$$

Here, $G_0 = 2e^2/h$ is the conductance quantum, f_C and f_A are the Fermi-Dirac distribution functions for the cathode and anode, respectively, and T is the transmission probability [22,23]. The latter is a total contribution of all subbands and can be expressed as

$$\begin{aligned} T(E) &= \sum_n T_n \\ &= \sum_n \left(1 + \exp\left\{-\frac{E - \left[\hbar\omega_y\,(n+1) + eV_0\right]}{\hbar\omega_x/2\pi}\right\}\right)^{-1}, \end{aligned} \tag{2}$$

where eV_0 is the potential energy at the bottleneck and ω_x and ω_y are frequencies related to the curvature of the potential, and thus of the shape of the constriction, along the axis of the filament and the transverse direction, respectively [24,25]. As one can see, the transmission of each individual subband varies from 0 to 1, meaning that the total transmission across the CF can be greater than that of any individual subband.

One can use the variables α to express the curvature of all subbands (which depends on the constriction length) and Φ_n to express the corresponding barrier height of the nth subband:

$$\alpha = \frac{2\pi}{\hbar\omega_x}, \tag{3}$$

$$\Phi_n = \hbar\omega_y\,(n + 1/2) + eV_0. \tag{4}$$

If one inserts these equations into Eq. (1) and assumes no smearing of the Fermi function, one obtains the following expression for the electrical current:

$$I = \frac{G_0}{e}\sum_n \left[eV + \alpha^{-1} \times \ln\left(\frac{1 + \exp\{\alpha\left[\Phi_n - \beta eV\right]\}}{1 + \exp\{\alpha\left[\Phi_n + (1-\beta)\,eV\right]\}}\right)\right]. \tag{5}$$

Here, β determines the location of the constriction, such that the Fermi level of the cathode is βeV above the Fermi level at the constriction and the Fermi level of the anode is $(1-\beta)\,eV$ below this point.

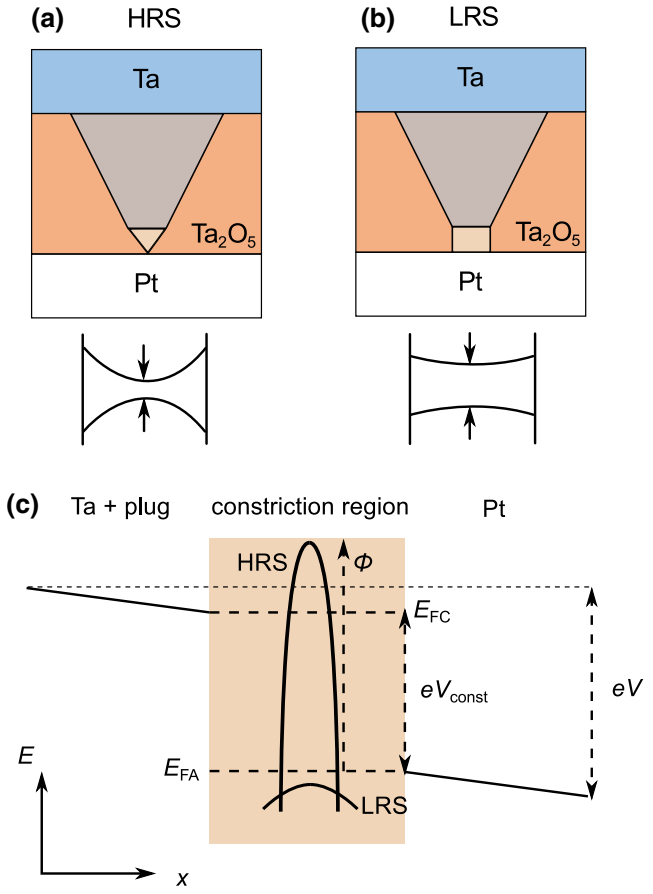

FIG. 1. (a),(b) Possible configurations of the conductive filament in the Pt/Ta/Ta_2O_5/Pt devices experimentally investigated in this work, showing the possible constriction at the Ta_2O_5-Pt interface for the HRS and LRS, respectively. Below the stack schematics, diagrams are shown of the corresponding analogous evolution of the constriction width between the HRS and the LRS. (c) The simplified energy (E) diagram of the resulting barrier for both states considering the SSA to the QPC model, highlighting the difference in the barrier height Φ. V is the total applied voltage, while $V_{\text{const}} = V - IR$ is the voltage drop across the constriction, with I the current and R the series resistance (which accounts for the resistance of the electrodes, wires, contacts, and the plug of the filament).

Some researchers [26–28] have considered an approximation to the QPC model where only the first subband contributes to the conduction, which is called the SSA. This is equivalent to stating that the energetic distance between subbands, $\hbar\omega_y$, is large enough so that the transmission through subbands beyond the first one is close to zero. One then considers that the conduction can occur over N parallel channels, such as different filaments or oxygen-vacancy paths. A single barrier height Φ is assumed, and the expression for the current can be reduced to

$$I = \frac{G_0}{e} N \left[eV + \frac{1}{\alpha} \ln \left(\frac{1 + \exp\{\alpha \left[\Phi - \beta eV\right]\}}{1 + \exp\{\alpha \left[\Phi + (1-\beta)\, eV\right]\}} \right) \right]. \tag{6}$$

Figure 1(c) displays a simplified band diagram of the resulting barrier at the constriction, while Figs. 1(a) and 1(b) schematically show a possible configuration of the constriction in the Pt/Ta/Ta_2O_5/Pt devices in the HRS and the LRS, respectively.

II. EXPERIMENTAL DETAILS

Several 10×10 μm^2 cross-point devices are investigated. The actual metal-insulator-metal (M-I-M) resistive switching structure consists of Pt/Ta/Ta_2O_5/Pt stacks. Figure 2 depicts the studied structure schematically. The Ta electrode in particular is meant to work as a scavenging layer, absorbing some oxygen from the oxide layer and creating additional oxygen vacancies [29]. The details of the sample preparation and geometry have been described elsewhere [30].

The electrical characterization is performed using a Keithley 2611A source meter. The cells are formed at room temperature with current-compliance (CC) values of 50 μA, 100 μA, 200 μA, and 1 mA, which are then used for the subsequent switching. Low CC values are used to study the case where the HRS and LRS overlap and whether the conduction mechanisms tested are consistent in this regime of operation. In order to avoid a hard breakdown in the samples, higher values are not employed. The samples are subjected to current-voltage (I-V) sweeps at a rate of about 0.3 V/s at room temperature. The voltage goes down to -1.5 V for the RESET operation. For the SET operation, the voltage is swept up to $V = V_{SET} + 0.25$ V, where V_{SET} is the voltage at which the CC is reached; this adaptive upper limit allows greater flexibility in setting the sweep parameters, without inducing unnecessary stress on the samples. For the representative data used in the analysis described here, a total of 1250 cycles are measured for each CC value in a single resistive switching device.

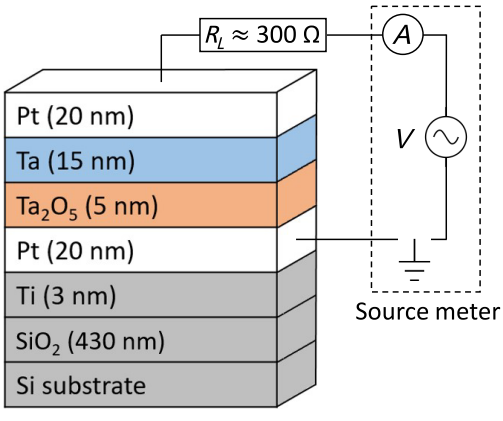

FIG. 2. A schematic representation of the ReRAM cells studied. A circuit diagram including the series resistance R_L and the source meter is also included.

Other devices from the same batch are tested to confirm the goodness of fit obtained with the SSA of the QPC but an extensive statistical analysis of the interdevice variability on the fitting parameters of the SSA is not conducted. From the results obtained, it seems that the cycle-to-cycle variability in a particular device, due to the stochasticity of the switching phenomenon, is already comparable with the variability between different devices and overshadows the conclusions that could be drawn from such an analysis.

III. RESULTS AND DISCUSSION

A. Resistive switching evaluation

Figure 3(a) shows the "intrinsic" switching of the device for the four CC values used. To display this "intrinsic" switching, the voltage drop across the metallic electrodes and wires, which act as a series resistance, is accounted for [31]. This process results in an apparent negative slope of the curve "during" the SET operation; this is merely a result of the way in which the data are displayed, as there are no data points in that interval of the curve (the line only aids in following the progression of the data), given the abrupt nature of the SET process. Bipolar RS can be observed in all cases. The Ta scavenging layer is expected to form an Ohmic contact with the plug, while the Pt bottom electrode should be where the disk is located [4,32]. Thus, one assumes that it is at this interface that the voltage drop across the device takes place. This means that the asymmetry parameter β takes the value of 1, which allows the removal of one variable from Eqs. (5) and (6).

The HRS and LRS statistics are depicted in Fig. 3(b). These are defined as the resistance values at 0.1 V for both device states. It can be seen that the mean value of the resistance in the HRS does not change significantly with increasing CC, experiencing only a slight decrease. All four distributions of the resistance in the HRS overlap significantly. On the other hand, the resistance in the LRS depends directly on the applied CC, as this is the limit on the current during the SET process. Its variability also tends to decrease with increasing CC. For CC < 200 μA, it can be seen that the two resistance-state distributions begin to overlap. This is an indication that conduction in

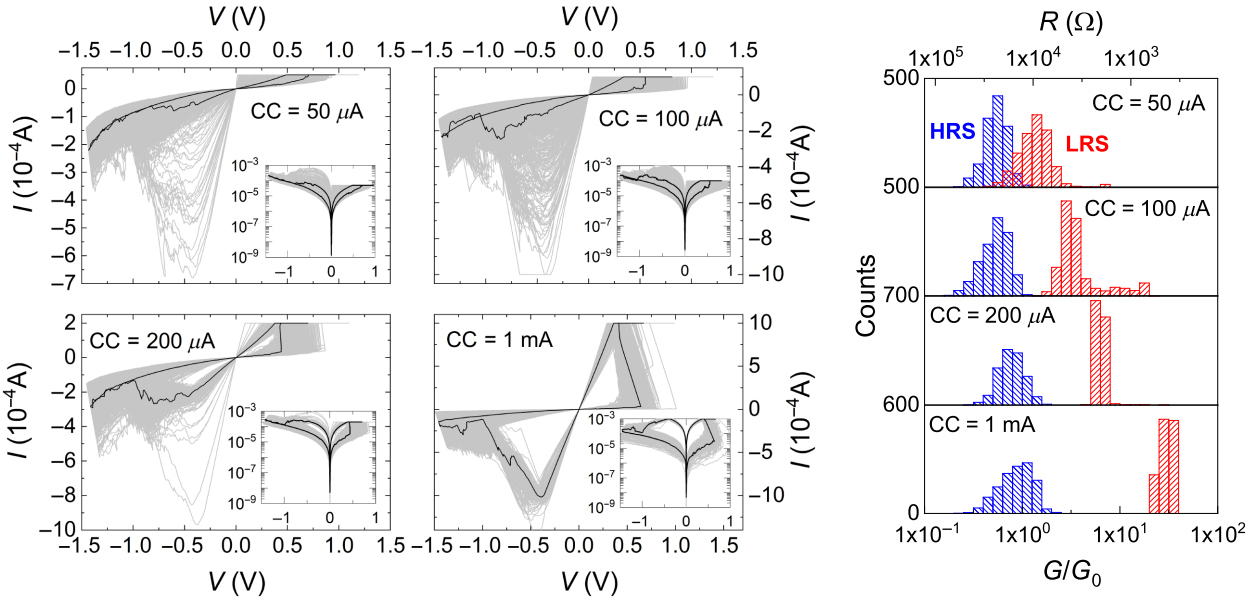

FIG. 3. (a) I-V sweeps during 1250 cycles for each CC value, highlighting a representative cycle for each set of curves. (b) The histogram of R_{HRS} and R_{LRS} for the 1250 I-V sweeps per CC value.

the HRS and LRS for low CC could be explained by the same conduction mechanisms.

B. Comparison of conduction models

The QPC and its SSA are initially applied via Newton's method for optimization [33]. However, we arrive at the conclusion that tight control over the starting parameters is needed, especially for the original model, to converge to a suitable solution. This makes this fitting method unsuitable for the volume of data that has to be analyzed. The fitting is then tried using a Gauss-Newton algorithm [33] and a Levenberg-Marquardt algorithm [33], with multiple heuristics developed for the regularization weight. For the details of the numerical methods, see Sec. S1 of the Supplemental Material [34]. It has been found that, for the SSA, this last approach is capable of producing adequate-quality fits, with a high degree of freedom regarding the initial fitting parameters. However, the original model cannot achieve such results for the whole data set with any of the methods used. Thus, the SSA is used to compare the QPC with other, more conventional, models.

The other conduction mechanisms considered are as follows: trap-assisted tunneling (TAT), Fowler-Nordheim (F-N) tunneling, Schottky emission, power-law expressions (Ohmic conduction, nearest-neighbor hopping, and variable-range hopping), Simmons modified Schottky emission (SMSE), and Poole-Frenkel (P-F) emission [35]. The respective mathematical expressions are linearized and linear fits to the experimental data in the linearized plots are conducted for both device states and all values of CC used. The I-V data used in the fitting procedure comprise the whole voltage range before the SET or RESET events. See the Supplemental Material [34] for the mathematical expressions used for the different models (Sec. S2) and for exemplary plots displaying the results of the fitting of the data to different conduction mechanisms (Fig. S1). The obtained coefficient-of-determination (R^2) statistics are depicted in Fig. 4. This coefficient is defined as

$$R^2 = 1 - \frac{R_{SS}}{S_{YY}}, \tag{7}$$

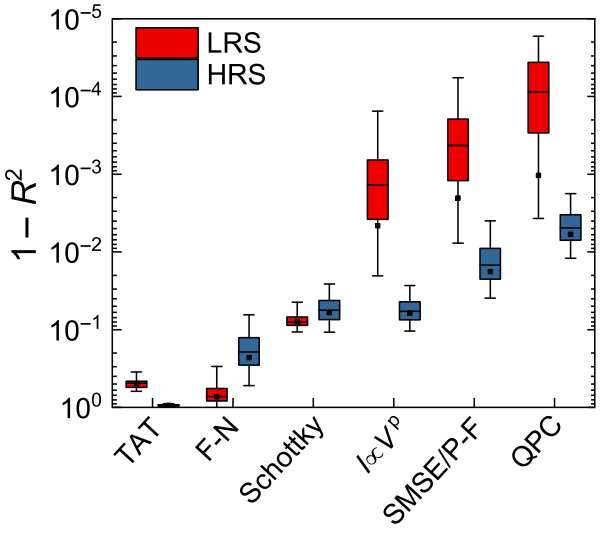

FIG. 4. (a) The R^2 statistics for all values of CC, separated by the device resistance state and model used for fitting. The lines denote the 5%–95% range of the distribution and the boxes 25%–75%, and the black square is the mean value.

where R_{SS} is the residual sum of squares and S_{YY} is the data variance for each fitting procedure [36].

Therefore, the plot in Fig. 4 shows the quality of the fit to the I-V data collected using the different conduction mechanisms, for the whole voltage range before SET or RESET events, for the entire set (1250 cycles) of all the different LRSs and HRSs.

The TAT and F-N tunneling are deemed to offer poor fitting quality for both device states. The Schottky emission and power-law expressions for the HRS offer poor predictive power, rapidly diverging from the experimental data as the voltage increases. Power-law expressions (including Ohmic behavior) result in good overall fits for the LRS, except for the lower values of CC, where this state exhibits a higher nonlinearity. P-F emission and SMSE provide good quality of fit for both device states. However, one can take the slope of the linearized curve, A, and obtain the relative permittivity of the device, $\sqrt{\varepsilon_r}$, via

$$r\sqrt{\varepsilon_r} = \frac{1}{A}\frac{e}{kT}\sqrt{\frac{e}{d\pi\varepsilon_0}}, \tag{8}$$

where T is the temperature, k is the Boltzmann constant, d is the oxide thickness, e is the electron charge, ε_0 is the vacuum permittivity, and r is a compensation factor so that $1 \leq r \leq 2$ [37].

From the available literature on tantalum oxide [38–48], the expected value for the relative permittivity is in the range $20 \leq \varepsilon_r \leq 40$, so that $4.47 \leq r\sqrt{\varepsilon_r} \leq 12.64$. The fitting parameters for the 5%–95% range are $12.93 \leq r\sqrt{\varepsilon_r} \leq 31.92$ and $20.18 \leq r\sqrt{\varepsilon_r} \leq 254.10$ for the HRS and LRS, respectively. Note that $d = 5$ nm is used but, as per the VCM model, this value should be smaller. The oxide barrier should be only the disk and the length of the plug should not be accounted for here. This correction would even further increase the obtained values of $r\sqrt{\varepsilon_r}$.

In this case, one must question whether the P-F emission and SMSE models, devised for conduction in highly insulating mediums, can still be regarded as the dominating conduction mechanism: it may be the case that the mathematical formula is merely providing an adequate phenomenological model [49]. In particular, for the LRS, one encounters the limit where $\varepsilon_r \to +\infty$ and the P-F equation converges to a power-law expression. This does not rule out the P-F emission or the SMSE as the main conduction mechanism in the HRS but it highlights the importance of searching for a model that provides both a good fit to the experimental data and a plausible physics-based explanation for the conduction.

The QPC, implemented with the SSA, shows the lowest mean value of $1 - R^2$, thus being the model that offers the best quality of fit to both the HRS and the LRS from the set of mechanisms considered. One important reason for the good quality of fit to the LRS is the capability of fitting not only linear but also nonlinear I-V characteristics. Roldán *et al.* have also shown, although with a different numerical analysis and for HfO_x-based devices, that P-F and F-N tunneling cannot explain the measured I-V curves, while the QPC reproduces the experimental behavior [50].

C. Validity of the SSA

The SSA hinges on the assumption that only the first subband contributes to the conduction. This assertion is tested by simulating the transmission for the first five subbands (as the contribution of higher values of n is very small) and the resulting total transmission (the conductance of the CF). The results, taken for different combinations of α and Φ_n, are displayed in Fig. 5.

As expected, when the energetic distance between subbands Φ_n is large, as seen in Figs. 5(a) and 5(b), the transmission can be considered to be mainly due to the first subband alone. Here, the approximation holds true. For wider barriers (high α), as seen in Fig. 5(c), if the applied voltage is high enough, one should observe discrete levels in the conductance, similarly to what is seen in two-dimensional electron-gas devices [51]. However, if the constriction is longer and the resulting energy barriers are thinner, one encounters the scenario represented in Fig. 5(d). Here, the approximation is no longer valid, as many subbands have a significant contribution to the transmission. Therefore, an issue arises, as one can emulate the total transmission by taking the curve for the first subband alone and adding an external multiplication factor:

$$T = \sum_n \frac{1}{1 + \exp\left[\alpha(\Phi_n - E)\right]} \approx \frac{N}{1 + \exp\left[\alpha(\Phi_1 - E)\right]}. \tag{9}$$

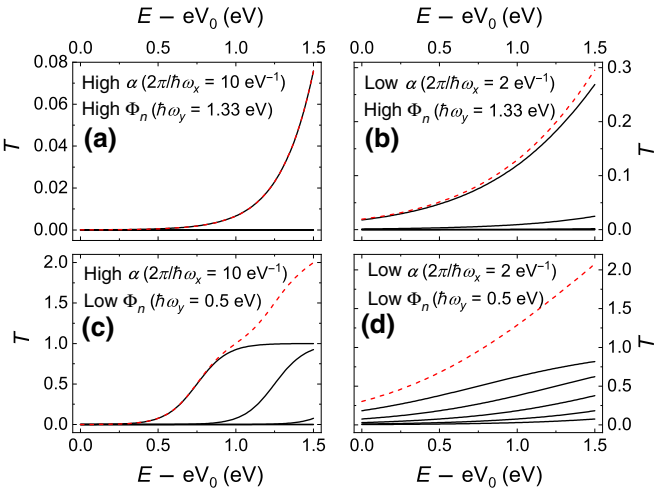

FIG. 5. The transmission for the first five subbands (black curves) and the total resulting transmission (red curves). Four combinations of α (related to the length of the constriction) and Φ_n (related to the width of the constriction) are considered.

This is equivalent to considering that the conduction occurs through multiple parallel paths, the interpretation given to the parameter N in the SSA [28]. Thus, one can see that the SSA should yield a good quality of fit in cases where it should not be applied: the value of N will be higher than expected, as an effective contribution of the neglected subbands is included in it. One should expect that the barrier height Φ will also be higher, while α, being constant for all subbands (as it is not directly involved in the energy quantization at the constriction), will also be constant for the total transmission curve. This suggests that great care needs to be taken when interpreting the results of the SSA, as a loss of physical accuracy may occur.

D. Single-subband-approximation results

Figure 6(a) shows the parameter N of the SSA fit versus the conductance measured at 0.1 V, normalized by the conductance quantum G_0. The two appear not to be strongly correlated in the HRS. In the LRS it can be seen that, at higher conductance values, the results tend to $N = G/G_0$, where the transmission of the first subband is equal to 1. Figure 6(b) shows the parameters α and Φ resulting from the application of the models, plotted versus each other. The color scale represents the transmission, as given by Eq. (9) once normalized by N, for an applied voltage of 0.1 V. The lines denote regions with the same transmission value. It can be seen that the product $\alpha\Phi$ appears to be constant. This result can be recovered from Eq. (9) in the limit when $E \to 0$.

For higher values of CC, the I-V characteristics tend to be highly linear in the LRS [Fig. 3(a)]. In some papers, the filament is said to display metallic conduction, while in others, evidence for very Ta-rich filaments is reported via detailed microscopic and spectroscopic techniques [11,13,14,52,53]. In this state, the SSA displays an advantage over the original model. In the latter, with the disappearance of the subband energy barriers that are expected in the LRS, the current tends to infinity:

$$I \to \frac{G_0}{e} \sum_{n=1} eV \xrightarrow[n\to+\infty]{} +\infty. \tag{10}$$

This results from the consideration of an infinite number of possible subbands in the model. In reality, conduction stops being ballistic in nature, as scattering effects become increasingly important and eventually dominate the conduction in the filament.

On the other hand, considering the SSA, the current tends to a finite limit value:

$$I \to NG_0V. \tag{11}$$

This is the expression for a linear resistor with $R = (NG_0)^{-1}$. This shows that the SSA returns a good quality of fit, even in the case where it is physically unfeasible

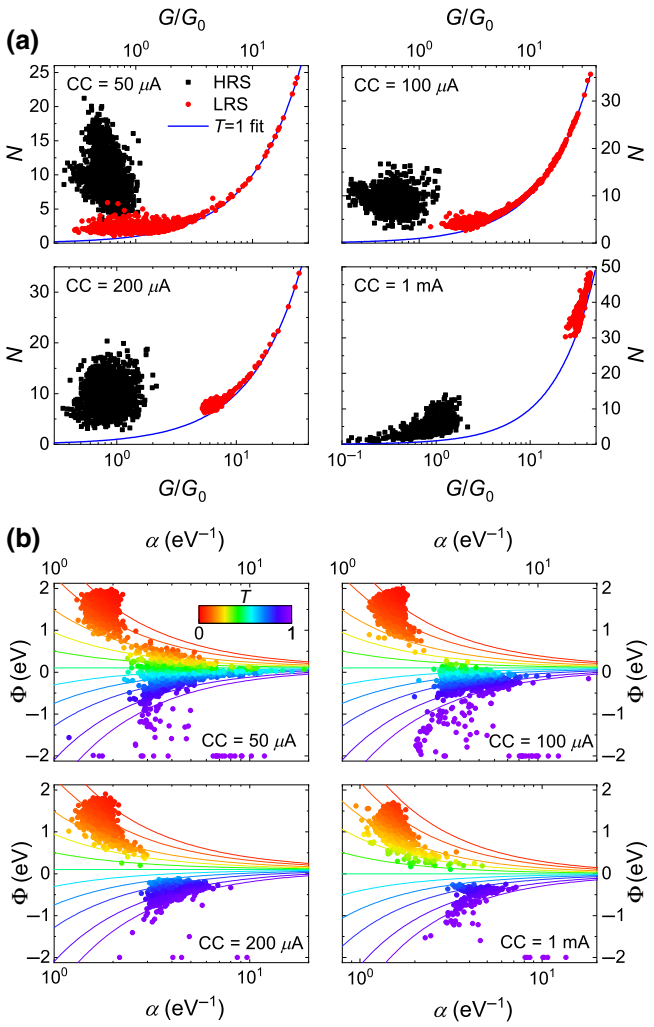

FIG. 6. (a) The values of N resulting from the application of the SSA, plotted versus the normalized conductance measured at 0.1 V. (b) The values of Φ versus α resulting from the application of the SSA, with a color scale representing the normalized transmission at 0.1 V.

to consider it. Consequently, the SSA can be used to simulate the response of the device quite accurately but care must be taken when attempting a physical interpretation of the results. Namely, the negative barrier-height values obtained from the fit mean that the barrier no longer presents a significant obstacle to conduction, as it lies below the quasi-Fermi level at the active electrode side, as shown for the LRS case in the scheme of Fig. 1(c).

Additionally, the SSA returns good results for more nonlinear LRS curves, which is predominantly the case for lower CC values. Even for a CC of 50 μA, where the conductance values in both device states overlap strongly, one can find distinctions in the parameters. It can be seen in Fig. 6(a) that the HRS tends to return higher values of N. In Fig. 6(b), it is visible that the HRS curves form a cluster at the top-left region of the graph, displaying higher

values of Φ and lower values of α than the LRS curves with similar conductance at 0.1 V. This indicates that the SSA is sensitive to small changes in the device behavior. More interestingly, it can provide a common explanation for the conduction in both device states. Starting with very low values of CC, the LRS is merely the result of a small softening in the constriction. As the conductance increases, the device behaves more linearly, with a decreasing Φ and increasing α indicating a reduction of the potential barrier.

Looking back at Fig. 6, it can be seen that, even for the lowest conductance values in the HRS, N tends to be greater than 1. This is true even for a higher CC of 1 mA, where N decreases more strongly with decreasing G/G_0. For these less-conductive states, α and Φ also tend not to display particularly high values, both being in the range of those proposed in Fig. 5(d). The conductance is also more strongly correlated with Φ than with α. These observations all point to the scenario presented in Fig. 5(d), where it is deemed that the SSA is invalid.

To reap the computational advantages that the SSA displays over the original model, one is thus forced to reinterpret the resulting parameters. As previously discussed, N should be looked at as an effective measure of the number of subbands that contribute to the conduction and Φ as an effective barrier height of these subbands. It is possible to infer the original variables ω_y and V_0 based on the results. High values of N indicate that the contribution of multiple subbands beyond the first, and thus the energy difference between them, related to ω_y, should be small. A higher or lower Φ should then be related to their distance to the Fermi level, V_0, but the value of Φ would also be influenced by more subbands of higher energy contributing to the conduction and thus to N. However, this is a less satisfactory way to model the conduction, as the new parameters N and Φ cannot be directly linked to the original properties of the physical system under study.

The SSA to the QPC should thus be looked at as a simplification of the original problem. The summation over multiple subbands is reduced to an overall effective contribution, facilitating its application but hindering its direct interpretation. Still, it allows us to make some analysis of the system, even if more qualitative, and it provides a good phenomenological model of the switching in the types of devices studied. Its use instead of the original model, or other more conventional models of conduction, will depend on the objectives of the analysis at hand.

E. Validity of the QPC model in the framework of VCM-based ReRAM

As discussed before, the SSA to the QPC model can provide an accurate fit of the I-V data of Pt/Ta/Ta_2O_5/Pt ReRAM devices. These devices exhibit characteristics typical of VCM-based resistive switching. However, there are certain characteristics of this kind of switching that do not seem to be compatible with the framework of the QPC model.

One such characteristic is the asymmetry in the I-V curves regarding the polarity of the applied voltage. Such asymmetry occurs normally in the HRS, or the LRS with high resistance (and also typically a more nonlinear I-V characteristic). This has been observed for similar ReRAM stacks based on TaO_x [7,32] but also for bilayer configurations [54]. Even though the asymmetry is not strong, for most of the cases it cannot be explained solely by the QPC method, as the transmission through the constriction is not polarity dependent. However, a possible origin of the observed asymmetries could be the interchange of oxygen species between the oxide layer and the Pt electrode, which is shown to impose a second resistive switching loop with opposite polarity in TiN/Ta_2O_5/Pt ReRAM devices [55]. This second (volatile) loop leads to an increase of the HRS resistance before the SET event, thus giving an asymmetry in the HRS I-V characteristics. The different work functions of the metal electrodes could also induce a small asymmetry.

Another characteristic of the VCM-type switching that is hard to envision through the QPC model is the bipolar behavior, i.e., SET occurring for a certain polarity of the applied voltage, while RESET occurs for the opposite polarity. If the SET or RESET operations are linked to the enlargement and shrinkage of a constriction, there is no reasonable explanation for the choice of the polarity for these changes in the constriction width. This can be largely overcome if one considers the case, as in the VCM model, of the modulation of the oxygen-vacancy content in the disk, as shown in Fig. 7. The HRS is linked to a lower concentration of oxygen vacancies in the disk region, as shown in Fig. 7(a). On the other hand, and following the same logic, the LRS is associated with a higher concentration of oxygen vacancies in the disk, as in Fig. 7(b). The lower concentration of vacancies in the HRS case possibly allows for fewer and isolated conduction paths through these vacancies, while in the LRS there is a higher number of possible conduction paths. This could be understood as the modulation of a constriction, as the higher number of conduction paths in the LRS could easily form a thicker conduction path, when compared to the fewer paths in the HRS. This interpretation should remain valid even if the conduction paths are not due to the presence of oxygen vacancies but, instead, of Ta granules, as our previous studies seem to point out [15]. Ta cations have been pointed out as mobile species in the Ta_2O_5 layer [56]. On the other hand, electron-microscopy studies in TiN/TaO_x/TiN structures show that the Soret diffusion of Ta could be the main driving force responsible for the formation of the filament [13,14]. This Soret diffusion occurs radially, i.e., perpendicularly to the filament. They also show the formation

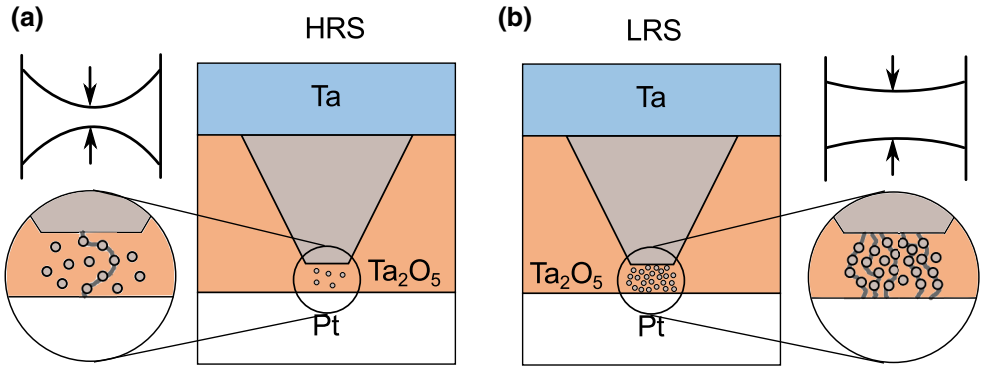

FIG. 7. A schematic depicting the possible reinterpretation of the constriction as conduction paths. (a) A lower concentration of the mobile species in the disk region would lead to a narrower constriction in the HRS. (b) A higher concentration of the mobile species in the disk region would lead to a less pronounced constriction or no constriction at all in LRS. The small circles represent the mobile species responsible for the modulation of the conductivity of the disk, e.g., oxygen vacancies or tantalum cations.

of the gap at one of the TaO_x-TiN interfaces (which one depends on the polarity of the forming voltage) and the existence of a subfilamentary path around the gap region (where there is crystallization of Ta_2O_5). This path is much narrower than the main part of the filament (the plug). Also, the conduction paths do not need to be physical, i.e., a connected path of a certain compound, as they could possibly be understood as a series of tunneling events between nonphysically connected conducting granules.

These alternative explanations could also be more compatible with the probable large current densities in the constriction region for the current values observed in the *I-V* characteristics in Fig. 3. For example, a current of 1 mA through a constriction region with a 50-nm-radius circular cross section would lead to a current density of approximately 10^7 A/cm^2. In the particular devices used for this work, the exact size of the conductive filaments is still an unsolved question, as no direct evidence for the dimensions of the conducting region in the oxide layer is obtained so far. The possible big impact of large current densities in the switching material could contradict some of the assumptions assumed when applying the QPC formalism.

On the other hand, the mathematical formalism behind the QPC, the Landauer-Büttiker formalism, involving the transmission between two "conduction reservoirs," is in fact more general, i.e., not necessarily involving a constriction. Funck *et al.* [57] have used a similar formalism in $SrTiO_3$-based ReRAM and ascribed the transport to tunneling through the Schottky barrier at the Pt-$SrTiO_3$ interface and band conduction in $SrTiO_3$. However, the switching is quite different than the one observed in the Pt/Ta/Ta_2O_5/Pt devices used in this work. Still, this points out that the compatibility of the QPC model with the experimental *I-V* data of ReRAM devices can be used with a different interpretation and not solely relying on a quantum constriction.

IV. CONCLUSIONS

Stable resistive switching typical of valence-change systems is obtained in Pt/Ta/Ta_2O_5/Pt samples and the measured *I-V* characteristics in the HRS and LRS are analyzed in the framework of the QPC model of conduction. The SSA is found to be more robust than the original QPC model and easier to apply in an automated fashion due to a weaker dependence on the starting guess. Both in the LRS and the HRS, the SSA to the QPC model provides a better fit than the other conduction mechanisms considered (Poole-Frenkel emission, Schottky emission, and Ohmic conduction, to list but a few).

The evolution of the SSA parameters when applied to the experimental data matches expectations, showing a lowering and widening of the energy barrier with an increasing filament conductance. It is found that, for higher conductance, the physical basis of the SSA no longer holds true but the mathematical model proves robust and capable of fitting such situations. Therefore, the first-subband approximation should be looked at as a simplification of the contribution of the multiple subbands. This allows a more reliable and efficient application of the QPC model to the experimental data but the loss in physical accuracy must be overcome by means of a more careful interpretation of the results and a closer focus on the qualitative rather than the quantitative analysis.

Beyond these problems, the general QPC approach faces challenges in explaining some typical characteristics of the resistive switching commonly accounted for via the valence-change mechanism. The simplistic view of a constriction with a change in its width does not seem to cope with some experimental observations. A reinterpretation of the physical meaning of the constriction in the context of the VCM could be helpful in this case. We argue that the change in the concentration of the mobile species in the disk region can influence the number of conduction paths through the disk, where a low concentration of

these species leads to a lower number of these paths, which should be equivalent to a narrower constriction. Apart from that, the mathematical formalism behind the QPC is rather general and can be interpreted in different ways.

In summary, we show that the QPC model with the single-subband approximation can fit the *I*-*V* characteristics of the ReRAM devices, especially in the HRS, being thus quite useful. Care must be taken, however, in the interpretation of the fitting parameters and in the conclusions to be drawn from the results.

ACKNOWLEDGMENTS

We would like to thank Alexander Schönhals for his help in the fabrication of the samples. This work was supported in part by project i3N, UIDB/50025/2020 and UIDP/50025/2020, financed by national funds through the Fundação para a Ciência e Tecnologia (FCT) and the Ministério da Educação e Ciência (MEC). J.M.M.A. and C.M.M.R. thank the FCT of Portugal for the studentships SFRH/BD/148189/2019 and PD/BD/105917/2014, respectively. N.A.S. acknowledges financial support from the Russian Science Foundation (Grant No. 21-19-00872, [67]) with respect to measuring the memristive properties. We thank the Deutsche Forschungsgemeinschaft (German Research Foundation, DFG) for financial support through the Collaborative Research Center SFB 917 "Nanoswitches." We also thank the Conselho de Reitores das Universidades Portuguesas (CRUP) and the Deutscher Akademischer Austauschdienst (German Academic Exchange Service, DAAD) for the Portuguese-German Integrated Action A-14/17.

[1] R. Waser, R. Dittmann, G. Staikov, and K. Szot, Redox-based resistive switching memories—nanoionic mechanisms, prospects, and challenges, Adv. Mater. **21**, 2632 (2009).

[2] M. J. Marinella and V. V. Zhirnov, in *Emerging Nanoelectronic Devices*, edited by A. Chen, J. Hutchby, V. Zhirnov, and G. Bourianoff (John Wiley & Sons, Chichester, 2015) 1st ed., Chap. 13, p. 246.

[3] I. Kataeva, F. Merrikh-Bayat, E. Zamanidoost, and D. Strukov, in *2015 International Joint Conference on Neural Networks (IJCNN)* (2015), p. 1.

[4] R. Waser, Redox-based resistive switching memories, J. Nanosci. Nanotechnol. **12**, 7628 (2012).

[5] S. Kim, S. Choi, and W. Lu, Comprehensive physical model of dynamic resistive switching in an oxide memristor, ACS Nano **8**, 2369 (2014).

[6] S. U. Sharath, M. J. Joseph, S. Vogel, E. Hildebrandt, P. Komissinskiy, J. Kurian, T. Schroeder, and L. Alff, Impact of oxygen stoichiometry on electroforming and multiple switching modes in TiN/TaO_x/Pt based ReRAM, Appl. Phys. Lett. **109**, 173503 (2016).

[7] C. E. Graves, N. Dávila, E. J. Merced-Grafals, S. T. Lam, J. P. Strachan, and R. S. Williams, Temperature and field-dependent transport measurements in continuously tunable tantalum oxide memristors expose the dominant state variable, Appl. Phys. Lett. **110**, 123501 (2017).

[8] Y. Wang, Y. Yan, C. Wang, Y. Chen, J. Li, J. Zhao, and C. S. Hwang, Controlling the thin interfacial buffer layer for improving the reliability of the Ta/Ta_2O_5/Pt resistive switching memory, Appl. Phys. Lett. **113**, 072902 (2018).

[9] F. Miao, J. P. Strachan, J. J. Yang, M. X. Zhang, I. Goldfarb, A. C. Torrezan, P. Eschbach, R. D. Kelley, G. Medeiros-Ribeiro, and R. S. Williams, Anatomy of a nanoscale conduction channel reveals the mechanism of a high-performance memristor, Adv. Mater. **23**, 5633 (2011).

[10] P. R. Mickel, A. J. Lohn, B. Joon Choi, J. Joshua Yang, M.-X. Zhang, M. J. Marinella, C. D. James, and R. Stanley Williams, A physical model of switching dynamics in tantalum oxide memristive devices, Appl. Phys. Lett. **102**, 223502 (2013).

[11] G. S. Park, Y. B. Kim, S. Y. Park, X. S. Li, S. Heo, M. J. Lee, M. Chang, J. H. Kwon, M. Kim, U. I. Chung, R. Dittmann, R. Waser, and K. Kim, *In situ* observation of filamentary conducting channels in an asymmetric Ta_2O_{5-x}/TaO_{2-x} bilayer structure, Nat. Commun. **4**, 2382 (2013).

[12] Y. Zhang, N. Deng, H. Wu, Z. Yu, J. Zhang, and H. Qian, Metallic to hopping conduction transition in Ta_2O_{5-x}/TaO_y resistive switching device, Appl. Phys. Lett. **105**, 063508 (2014).

[13] Y. Ma, D. Li, A. A. Herzing, D. A. Cullen, B. T. Sneed, K. L. More, N. T. Nuhfer, J. A. Bain, and M. Skowronski, Formation of the conducting filament in TaO_x-resistive switching devices by thermal-gradient-induced cation accumulation, ACS Appl. Mater. Interfaces **10**, 23187 (2018).

[14] Y. Ma, J. M. Goodwill, D. Li, D. A. Cullen, J. D. Poplawsky, K. L. More, J. A. Bain, and M. Skowronski, Stable metallic enrichment in conductive filaments in TaO_x-based resistive switches arising from competing diffusive fluxes, Adv. Electron. Mater. **5**, 1800954 (2019).

[15] C. M. Rosário, B. Thöner, A. Schönhals, S. Menzel, A. Meledin, N. P. Barradas, E. Alves, J. Mayer, M. Wuttig, R. Waser, N. A. Sobolev, and D. J. Wouters, Metallic filamentary conduction in valence change-based resistive switching devices: The case of TaO_x thin film with $x \sim 1$, Nanoscale **11**, 16978 (2019).

[16] S. Privitera, G. Bersuker, B. Butcher, A. Kalantarian, S. Lombardo, C. Bongiorno, R. Geer, D. C. Gilmer, and P. D. Kirsch, Microscopy study of the conductive filament in HfO_2 resistive switching memory devices, Microelectron. Eng. **109**, 75 (2013).

[17] E. Miranda and J. Suñé, in *2001 IEEE International Reliability Physics Symposium Proceedings* (IEEE, Orlando, Florida, 2001), p. 367.

[18] R. Degraeve, A. Fantini, S. Clima, B. Govoreanu, L. Goux, Y. Y. Chen, D. J. Wouters, P. Roussel, G. S. Kar, G. Pourtois, S. Cosemans, J. A. Kittl, G. Groeseneken, M. Jurczak, and L. Altimime, Dynamic "hour glass" model for SET and RESET in HfO_2 RRAM, Digest of Technical Papers—Symposium on VLSI Technology, 75 (2012).

[19] J. van Ruitenbeek, M. M. Masis, and E. Miranda, in *Resistive Switching*, edited by D. Ielmini and R. Waser (Wiley-VCH Verlag, Weinheim, 2016), Chap. 7, p. 197.

[20] R. Landauer, Spatial variation of currents and fields due to localized scatterers in metallic conduction, IBM J. Res. Dev. **1**, 223 (1957).

[21] M. Buttiker, Four-Terminal Phase-Coherent Conductance, Phys. Rev. Lett. **57**, 1761 (1986).

[22] P. Hu, One-dimensional quantum electron system under a finite voltage, Phys. Rev. B **35**, 4078 (1987).

[23] M. Büttiker, Quantized transmission of a saddle-point constriction, Phys. Rev. B **41**, 7906 (1990).

[24] J. N. L. Connor, On the analytical description of resonance tunnelling reactions, Mol. Phys. **15**, 37 (1968).

[25] W. H. Miller, Semiclassical treatment of multiple turning-point problems—phase shifts and eigenvalues, J. Chem. Phys. **48**, 1651 (1968).

[26] E. A. Miranda, C. Walczyk, C. Wenger, and T. Schroeder, Model for the resistive switching effect in HfO_2 MIM structures based on the transmission properties of narrow constrictions, IEEE Electron Device Lett. **31**, 609 (2010).

[27] X. Lian, X. Cartoixà, E. Miranda, L. Perniola, R. Rurali, S. Long, M. Liu, and J. Suñé, Multi-scale quantum point contact model for filamentary conduction in resistive random access memories devices, J. Appl. Phys. **115**, 244507 (2014).

[28] X. Lian, M. Wang, M. Rao, P. Yan, J. J. Yang, and F. Miao, Characteristics and transport mechanisms of triple switching regimes of TaO_x memristor, Appl. Phys. Lett. **110**, 173504 (2017).

[29] F. De Stefano, M. Houssa, V. V. Afanasev, J. A. Kittl, M. Jurczak, and A. Stesmans, Nature of the filament formed in HfO_2-based resistive random access memory, Thin Solid Films **533**, 15 (2013).

[30] C. Rosário, B. Thöner, A. Schönhals, S. Menzel, M. Wuttig, R. Waser, N. Sobolev, and D. Wouters, Correlation between the transport mechanisms in conductive filaments inside Ta_2O_5-based resistive switching devices and in substoichiometric TaO_x thin films, Appl. Phys. Lett. **112**, 213504 (2018).

[31] A. Fantini, D. J. Wouters, R. Degraeve, L. Goux, L. Pantisano, G. Kar, Y. Y. Chen, B. Govoreanu, J. A. Kittl, L. Altimime, and M. Jurczak, in *2012 4th IEEE International Memory Workshop (IMW)* (Milan, 2012), p. 1.

[32] W. Kim, S. Menzel, D. J. Wouter, Y. Guo, J. Robertson, B. Roesgen, R. Waser, and V. Rana, Impact of oxygen exchange reaction at the Ohmic interface in Ta_2O_5-based ReRAM devices, Nanoscale **8**, 17774 (2016).

[33] P. E. Gill, W. Murray, and M. H. Wright, *Practical Optimization* (Academic Press, London, 1981).

[34] See the Supplemental Material at http://link.aps.org/supplemental/10.1103/PhysRevApplied.17.034062 for details on the numerical methods implemented to fit the QPC model to the data and on the comparison of the QPC model with other conduction mechanisms, which includes Refs. [58–66].

[35] F.-C. Chiu, A review on conduction mechanisms in dielectric films, Adv. Mater. Sci. Eng. **2014**, 578168 (2014).

[36] A.-N. Spiess and N. Neumeyer, An evaluation of R^2 as an inadequate measure for nonlinear models in pharmacological and biochemical research: A Monte Carlo approach, BMC Pharmacol. **10**, 6 (2010).

[37] J. R. Yeargan and H. L. Taylor, The Poole-Frenkel effect with compensation present, J. Appl. Phys. **39**, 5600 (1968).

[38] L. Young and R. M. Barrer, The determination of the thickness, dielectric constant, and other properties of anodic oxide films on tantalum from the interference colours, Proc. R. Soc. London. Ser. A. Math. Phys. Sci. 244, 41 (1958).

[39] D. Husted, L. Gruss, and T. Mackus, Electrical properties of anodic oxide films of Ta, Nb, Zr, Ti, W, and V formed by the ion-cathode method, J. Electrochem. Soc. **118**, 1989 (1971).

[40] G. Aygun and R. Turan, Electrical and dielectrical properties of tantalum oxide films grown by Nd:YAG laser assisted oxidation, Thin Solid Films **517**, 994 (2008).

[41] P. S. Wilcox and W. D. Westwood, Anodic oxidation of tantalum, Can. J. Phys. **49**, 1543 (1971).

[42] D. J. Smith and L. Young, Optical and electrical properties of thermal tantalum oxide films on silicon, IEEE Trans. Electron. Devices **28**, 22 (1981).

[43] Y. Nakagawa and T. Okada, Material constants of new piezoelectric Ta_2O_5 thin films, J. Appl. Phys. **68**, 556 (1990).

[44] S. Zaima, T. Furuta, Y. Yasuda, and M. Iida, Preparation and properties of Ta_2O_5 films by LPCVD for ULSI application, J. Electrochem. Soc. **137**, 1297 (1990).

[45] K. Kukli, M. Ritala, and M. Leskelä, Atomic layer epitaxy growth of tantalum oxide thin films from Ta $(OC_2\ H_5)_5$ and H_2O, J. Electrochem. Soc. **142**, 1670 (1995).

[46] R. A. B. Devine, L. Vallier, J. L. Autran, P. Paillet, and J. L. Leray, Electrical properties of Ta_2O_5 films obtained by plasma enhanced chemical vapor deposition using a TaF_5 source, Appl. Phys. Lett. **68**, 1775 (1996).

[47] N. Inoue, T. Ozaki, T. Monnaka, S. Kashiwabara, and R. Fujimoto, A new pulsed laser deposition method using an aperture plate, Jpn. J. Appl. Phys. **36**, 704 (1997).

[48] W. S. Lau, L. Zhong, A. Lee, C. H. See, T. Han, N. P. Sandler, and T. C. Chong, Detection of defect states responsible for leakage current in ultrathin tantalum pentoxide (Ta_2O_5) films by zero-bias thermally stimulated current spectroscopy, Appl. Phys. Lett. **71**, 500 (1997).

[49] H. Schroeder, Poole-Frenkel-effect as dominating current mechanism in thin oxide films—an illusion?!, J. Appl. Phys. **117**, 215103 (2015).

[50] J. B. Roldán, E. Miranda, G. González-Cordero, P. García-Fernández, R. Romero-Zaliz, P. González-Rodelas, A. M. Aguilera, M. B. González, and F. Jiménez-Molinos, Multivariate analysis and extraction of parameters in resistive RAMs using the quantum point contact model, J. Appl. Phys. **123**, 014501 (2018).

[51] B. J. Van Wees, H. Van Houten, C. W. Beenakker, J. G. Williamson, L. P. Kouwenhoven, D. Van Der Marel, and C. T. Foxon, Quantized Conductance of Point Contacts in a Two-Dimensional Electron Gas, Phys. Rev. Lett. **60**, 848 (1988).

[52] M. K. Yang, H. Ju, G. H. Kim, J. K. Lee, and H. C. Ryu, Direct evidence on Ta-metal phases igniting resistive switching in TaO_x thin film, Sci. Rep. **5**, 14053 (2015).

[53] J. P. Strachan, G. Medeiros-Ribeiro, J. J. Yang, M. X. Zhang, F. Miao, I. Goldfarb, M. Holt, V. Rose, and R. S. Williams, Spectromicroscopy of tantalum oxide memristors, Appl. Phys. Lett. **98**, 242114 (2011).

[54] M.-J. Lee, C. B. Lee, D. Lee, S. R. Lee, M. Chang, J. H. Hur, Y.-B. Kim, C.-J. Kim, D. H. Seo, S. Seo, U.-I. Chung, I.-K. Yoo, and K. Kim, A fast, high-endurance and scalable non-volatile memory device made from asymmetric Ta_2O_{5-x}/TaO_{2-x} bilayer structures, Nat. Mater. **10**, 625 (2011).

[55] A. Schoenhals, C. M. M. Rosário, S. Hoffmann-Eifert, R. Waser, S. Menzel, and D. J. Wouters, Role of the electrode material on the RESET limitation in oxide ReRAM devices, Adv. Electron. Mater. **4**, 1700243 (2018).

[56] A. Wedig, M. Luebben, D. Y. Cho, M. Moors, K. Skaja, V. Rana, T. Hasegawa, K. K. Adepalli, B. Yildiz, R. Waser, and I. Valov, Nanoscale cation motion inTaO_x, HfO_x and TiO_x memristive systems, Nat. Nanotechnol. **11**, 67 (2016).

[57] C. Funck, A. Marchewka, C. Bäumer, P. C. Schmidt, P. Müller, R. Dittmann, M. Martin, R. Waser, and S. Menzel, A theoretical and experimental view on the temperature dependence of the electronic conduction through a Schottky barrier in a resistively switching $SrTiO_3$-based memory cell, Adv. Electron. Mater. **4**, 1800062 (2018).

[58] M. Avriel, *Nonlinear Programming: Analysis and Methods*, (Dover Publications, Mineola, New York, 2003), 1st ed., Chap. XIII, p. 288.

[59] C. T. Kelley, *Iterative Methods for Optimization* (Society for Industrial and Applied Mathematics, 1999), Chaps. 2, 3, 4, pp. 13, 39, 71.

[60] P. E. Gill and W. Murray, Algorithms for the solution of the nonlinear least-squares problem, SIAM J. Numer. Anal. **15**, 977 (1978).

[61] J. Pujol, The solution of nonlinear inverse problems and the Levenberg-Marquardt method, Geophysics **72**, W1 (2007).

[62] K. Levenberg, A method for the solution of certain nonlinear problems in least squares, Quarterly Appl. Math. **2**, 164 (1944).

[63] D. W. Marquardt, An algorithm for least-squares estimation of nonlinear parameters, J. Soc. Ind. Appl. Math. **11**, 431 (1963).

[64] M. Kuhn and K. Johnson, *Applied Predictive Modeling* (Springer, New York, 2013), p. 61.

[65] G. H. Golub, M. Heath, and G. Wahba, Generalized cross-validation as a method for choosing a good ridge parameter, Technometrics **21**, 215 (1979).

[66] E. W. Lim and R. Ismail, Conduction mechanism of valence change resistive switching memory: A survey, Electronics **4**, 586 (2015).

[67] https://rscf.ru/project/21-19-00872/